Module 2

Complex species in the core and edge of the fusion plasma. Describing and calculating their characteristics - the current state.

Lecture viewgraphs

Hugh Summers, Martin O'Mullane and Alessandra Giunta

University of Strathclyde

Contents

1.1 Key ADAS data formats

- *adf04*: A specific ion file is sufficient for the calculation of the excited populations of an ion. It is complete in itself, with energy levels and rate coefficients spanning a set of states beginning with the ground level.
- *adf11*: A set of element master files is sufficient for the calculation of the ionisation state of an element, that is the fractional abundances of the ions of the element and their radiated power.
- *adf15*: A photon emissivity coefficient file contains the predicted emissivity coefficients of a set of spectrum lines of an ion, spanned by an adf04 dataset, as a function of plasma parameters Te and Ne . Combined with the ionisation state above, it allows prediction of absolute spectral line emissivities.
- *adf40*: A feature photon emissivity file is the photon emissivity coefficient per pixel in a pixellated spectral range as a function of plasma parameters Te and Ne, due to all the spectrum lines of an ion spanned by an adf04 dataset. It is a construct for the efficient handling of a complex ion which may have hundreds of thousands of spectral lines.

1.2 Feature photon emissivity coefficients, $\mathcal{FPEC}$.

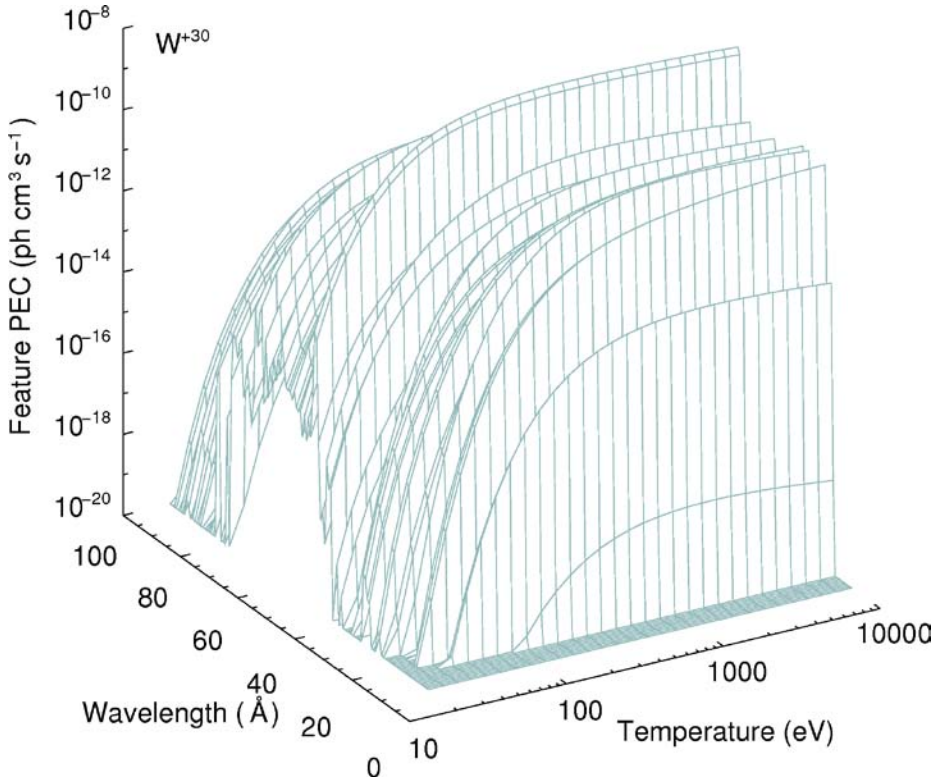

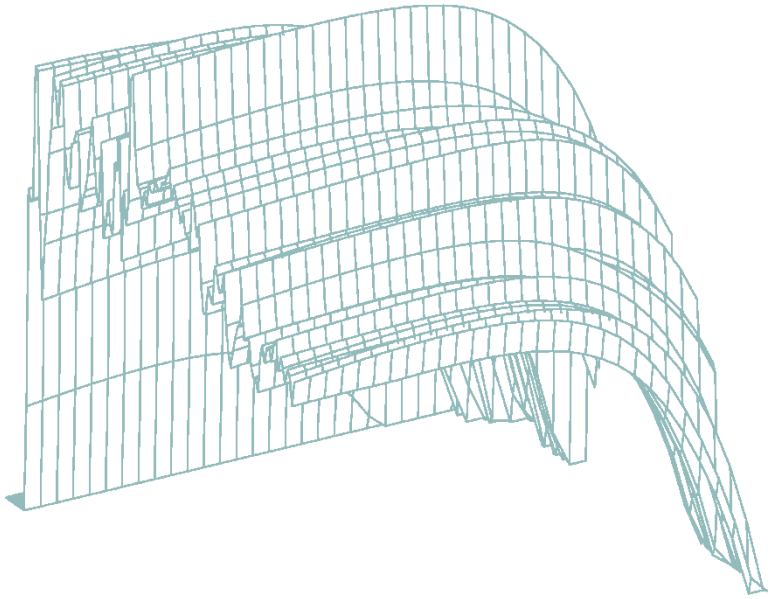

$\mathcal{FPEC}$ for W^{+20} in the spectral range of the XUV ('SOXMOS' - KT4) spectrometer at the JET facility versus electron temperature at the fixed electron density of 10^{+13} cm^{-3}. (a) View from the low temperature side. (b) View from the high temperature side showing the broadening into an envelope feature (see ADAS810).

1.3 Configuration string representations

Configuration string: $\Gamma \equiv n_1 l_1^{q_1} n_2 l_2^{q_2} \cdots n_m l_m^{q_m}$

Cowan form: $1s2\ 2s2\ 2p6\ 3s2\ 3p6\ 3d10\ 4s2\ 4p6\ 4d10\ 4f13\ 5s2\ 5p6$

Standard form: $1s2\ 2s2\ 2p6\ 3s2\ 3p6\ 3da\ 4s2\ 4p6\ 4da\ 4fd\ 5s2\ 5p6$

alphabetic

10 ≡a , 11 ≡b , 12 ≡c , 13 ≡d , 14 ≡e .

Standard coding

Eissner form: $52152256352456560652756860963A52B56C$

$2152256352456560652756860963A52B56C$

Leading 5 omitted

1 ≡1s , 2 ≡2s , 3 ≡2p , 4 ≡3s , 5 ≡3p , 6 ≡3d , 7 ≡4s , 8 ≡4p ,
9 ≡4d , A ≡4f , B ≡5s , C ≡5p , D ≡5d , E ≡5f , F ≡5g .

Eissner coding

Use *read_adf00.pro* to obtain the ground configurations of ions. Use *xxcftr.pro* to convert between standard and Eissner configuration forms.

1.4 The adf04 data format

There are five types of adf04 dataset:

1 – coll. strength v X

2 – currently not in use

3 – Maxwellian. aver. coll. strength v Te

4 – non-Maxwellian ups/downsilon v <energy>

5 – coll. strength v final state energy.

The level description field is free for the use of the adf04 dataset creator. With the move to heavier species and the very large automatic production of fundamental data for the ADAS/ADAS-EU projects, the descriptor is used for the configuration string.

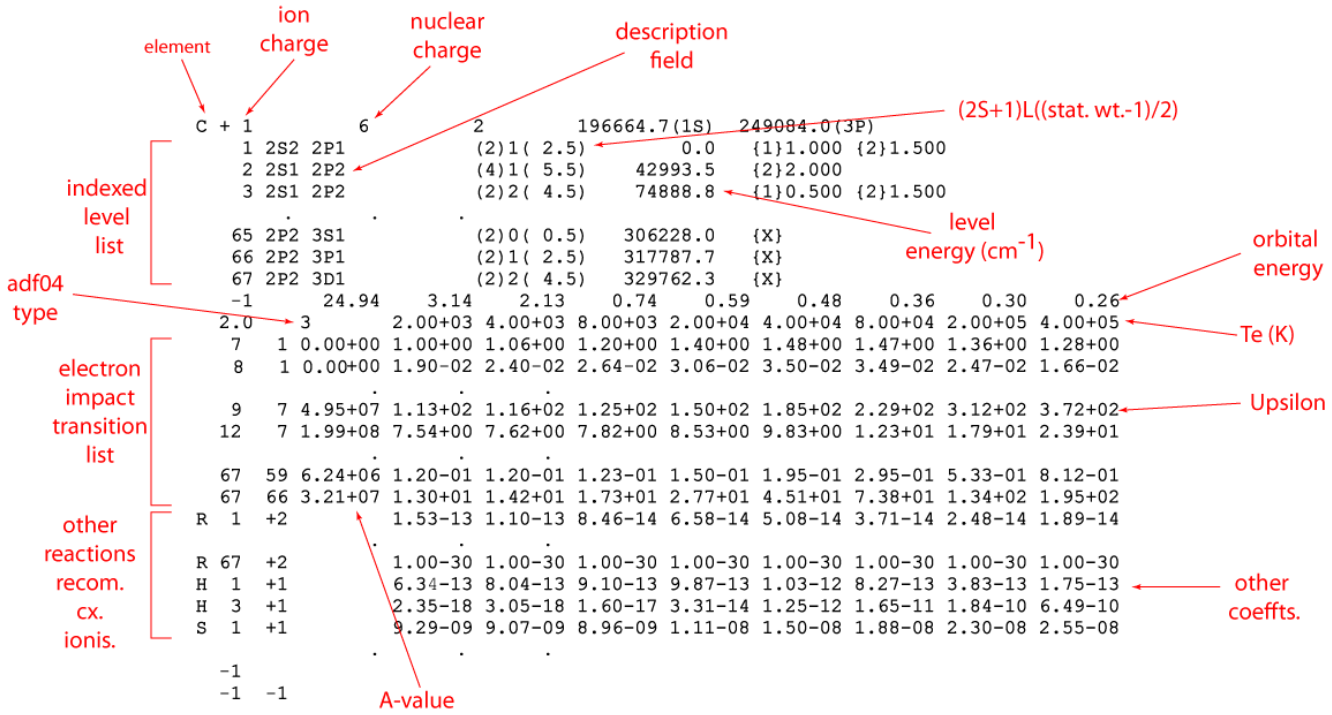

There are ~ 3500 adf04 datasets in the ADAS database in iso-electronic and iso-nuclear collections. These include preferred collections, fully expanded with supplementary reaction data. The adf04 collection is expanding rapidly with the heavy species production (see module 7).

1.5 W^{+9} adf04 datasets of different resolution

Portions of the level lists at the top of four adf04 datasets for the same ion, W^{+9}, are shown.

ADAS works with adf04 datasets of different resolution:
ca – config. resolution
ls – term resolution
ic – level resolution

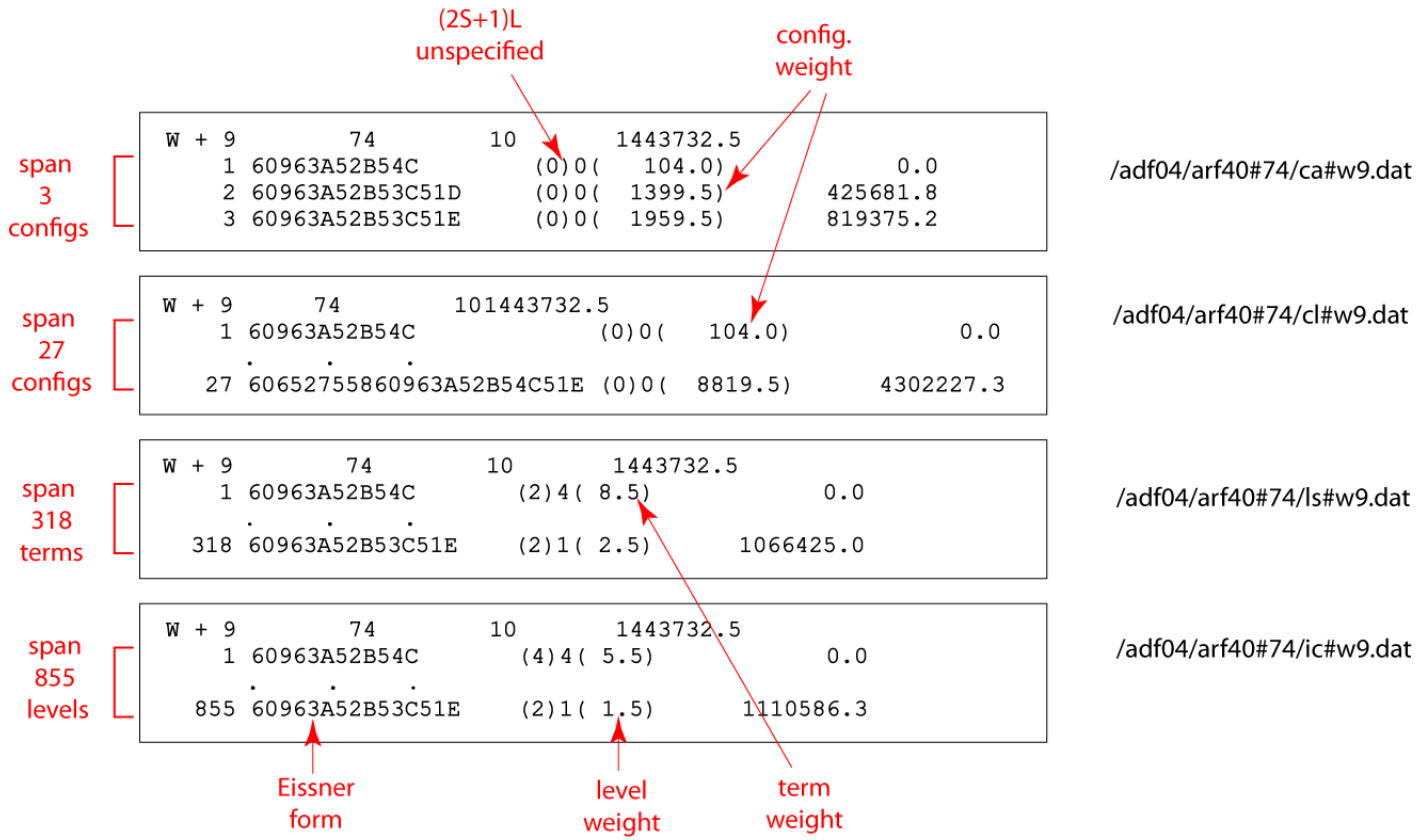

The first dataset is a small *ca* case with 3 configurations. These three configuration have 318 terms given in the third dataset (which is *ls*) and 855 levels given in the fourth dataset (which is *ic*). The fourth dataset yields a population solution of much higher precision. The second dataset is a large ca case with 27 configurations. It has large coverage but at low resolution. In *ic* it would span >10000 levels and overwhelm computers.

1.6 Assembling the high precision *ic* adf04 dataset

The schematic shows the inter-connected production codes and pathways which are used to form *adf04* datasets for light and medium weight ions of elements at the highest precision.

The ADAS codes containing '#' are non-interactive offline-adas codes executed in distributed processing by script. Available in ADAS, they require setting up for a specific site and multi-node computing environments. The methodologies and operation of these codes is described in module 7.

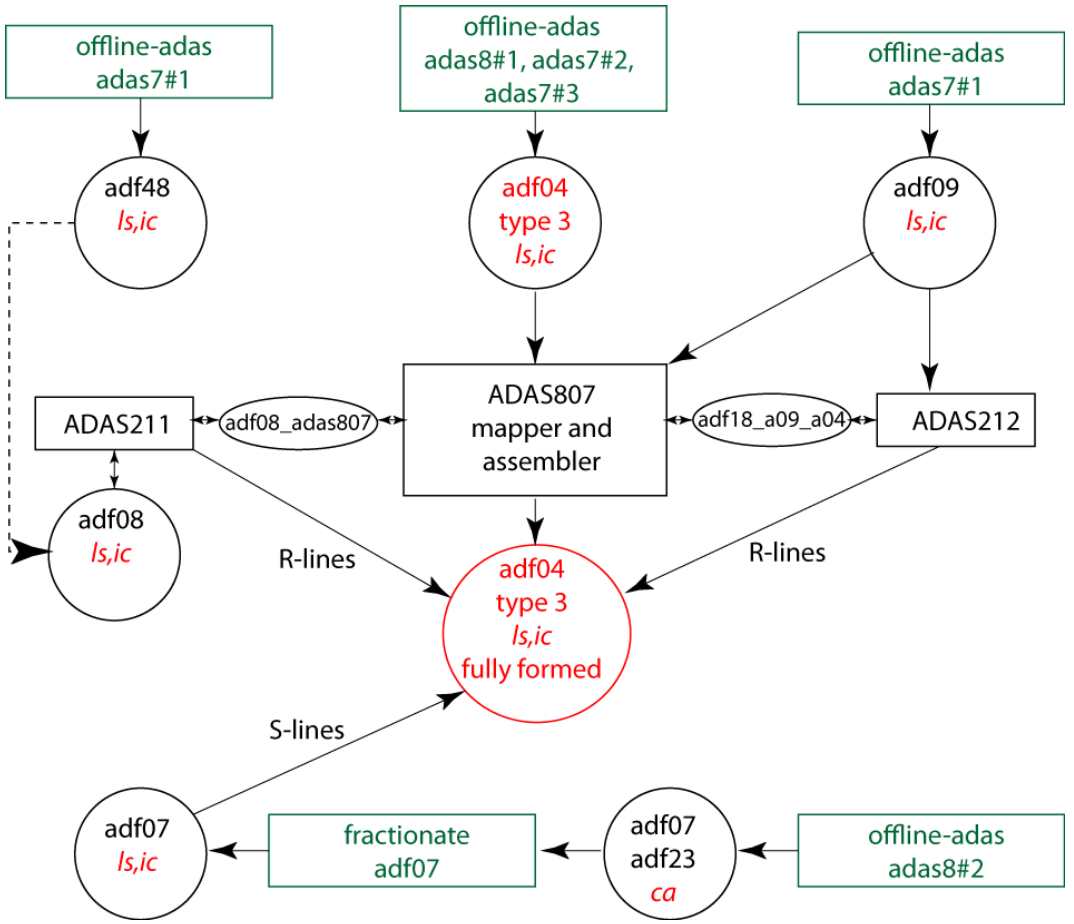

Codes in black letter capitals are part of interactive ADAS . Their use is included in the tutorial materials and example sheets presented at the full ADAS training course and are available from the ADAS and ADAS-EU websites. ADAS staff will be available after the ADAS-EU workshop to give further guidance.

2.1 Exploiting completeness and precision of adf04 datasets

The production of the *ca*, *cl*, *ls* and *ic* categories of *adf04* dataset has been automated for any element. This is done in multi-node distributed computation for all the ions of an element at the one time, optimised for precision in total radiated power. It has been particularly useful for creating the ADAS baseline for heavy species.

For the above purposes, the schematic outlines how the categories of *adf04* datasets are exploited, processing through to baseline *adf11* (see ADAS407 and ADAS408).

A more sophisticated procedure called bn-ls projection , also requiring the *adf04*, datasets has been used for the light elements. It is being extended to argon with completion so-far to silicon.

Current large scale, high precision *adf04* and other fundamental data production is in support of a new bnl-ic projection procedure for use through to zinc/zinc-like and selectively thereafter (see section 2 of module 2).

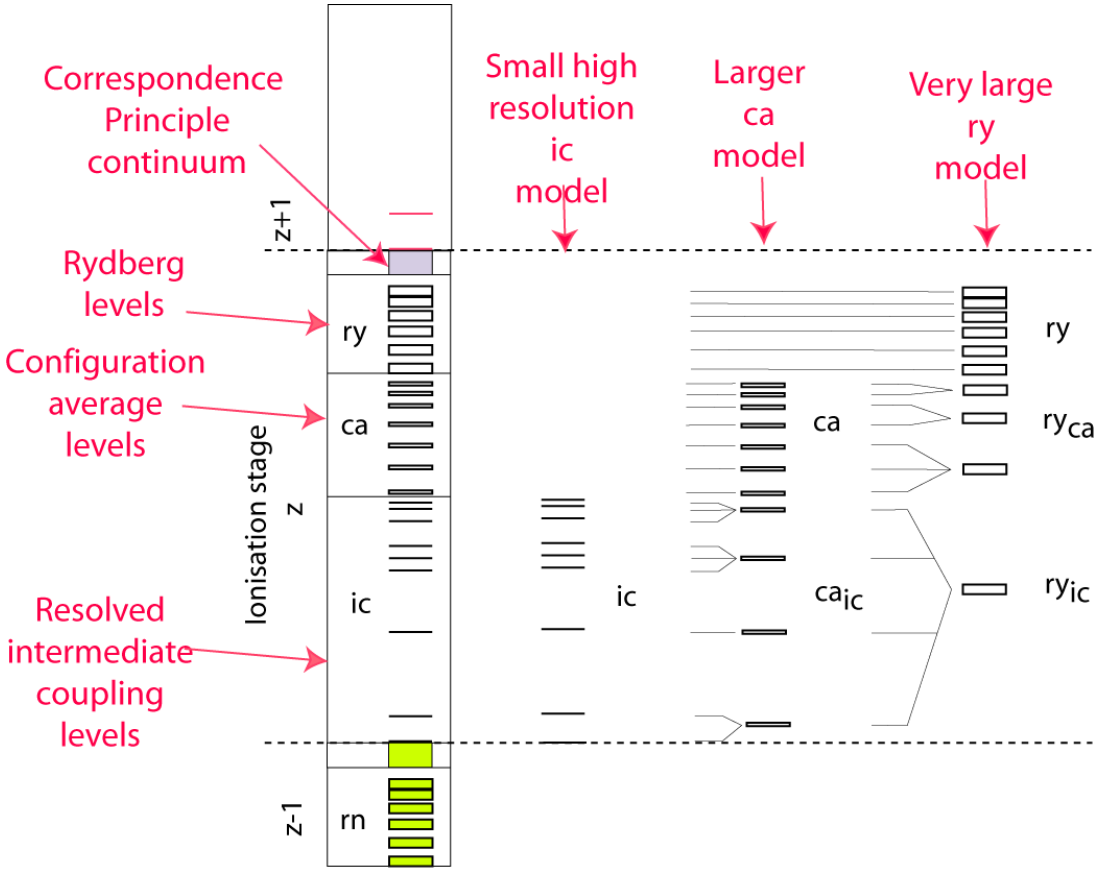

Yields a series of population calculations of varying resolution and span

Hence Power $P = P_{ic} + (P_{ca+ca_{ic}} - P_{ca_{ic}}) + (P_{ry+ry_{ca}+ry_{ic}} - P_{ry_{ca}+ry_{ic}})$

ca top-up ry top-up

2.2 Projection and condensation

For precision with light/medium weight elements, we have not dealt carefully enough with the truncation problem of the true atom with its infinite number of Rydberg states.

The study of dielectronic recombination of module 1 showed the importance of high Rydberg states and true population solutions for it with the bundle-n and bundle-nl models. So these models should be used to fill in the gap.

The matrix method used in module 1 to obtain the CR and GCR coefficients can be used again, as shown in the schematic, and again repeatedly.

Setup the bundle-n collisional-radiative matrix for the whole system. Use the inverse sub-matrix propagator for the ry n-shells to project onto the ry_{ca} and ry_{ic} n-shells. Eliminate the direct couplings and expand statistically over the ca and ca_{ic} nl-shell substructure and add to the more exact collisional-radiative matrix for ca + ca_{ic}

Repeat down to the high precision ic collisional-radiative matrix we need for spectroscopy.

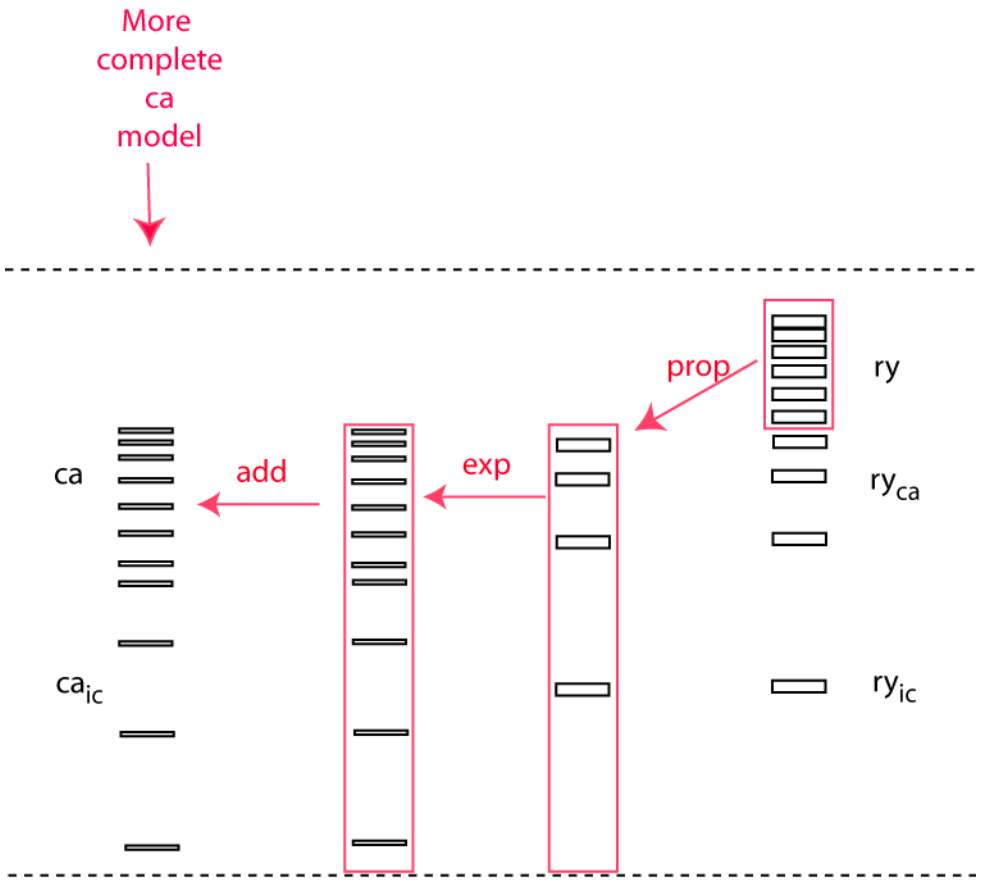

ry collisional-radiative matrix propagated onto the $ry_{ca} + ry_{ic}$ manifold, expanded over the higher resolution $ca + ca_{ic}$ manifold and added to the direct $ca + ca_{ic}$ collisional-radiative matrix.

2.3 Algebra of projection

Collisional-radiative matrices of progressively greater span (all *ic* levels, all *ca* levels, all *bn* levels) but lower resolution.

$$\left[\ C^{(ic)}_{i\,j}\ \right], \left[\begin{array}{cc} C^{(ca)}_{\bar{i}\,\bar{j}} & C^{(ca)}_{\bar{i}\,\bar{j}'} \\ C^{(ca)}_{\bar{i}'\,\bar{j}} & C^{(ca)}_{\bar{i}'\,\bar{j}'} \end{array}\right], \left[\begin{array}{ccc} C^{(bn)}_{\bar{\bar{i}}\,\bar{\bar{j}}} & C^{(bn)}_{\bar{\bar{i}}\,\bar{j}'} & C^{(bn)}_{\bar{\bar{i}}\,j''} \\ C^{(bn)}_{\bar{i}'\,\bar{\bar{j}}} & C^{(bn)}_{\bar{i}'\,\bar{j}'} & C^{(bn)}_{\bar{i}'\,j''} \\ C^{(bn)}_{i''\,\bar{\bar{j}}} & C^{(bn)}_{i''\,\bar{j}'} & C^{(bn)}_{i''\,j''} \end{array}\right]$$

not bundled

bundled over outer quantum numbers

bundled to n-shells

projected on to ic span

$$C^{(ca)}_{\bar{i}\,\bar{j}} \longrightarrow \bar{C}^{(ca)}_{\bar{i}\,\bar{j}} \qquad \bar{\bar{C}}^{(ca)}_{\bar{i}\,\bar{j}} = \bar{C}^{(ca)}_{\bar{i}\,\bar{j}} - C^{(ca)}_{\bar{i}\,j'}\left(C^{(ca)}_{j'\,i'}\right)^{-1} C^{(ca)}_{i'\,\bar{j}}$$

ic span

remove direct couplings

ca span

$$C^{(ic)}_{i\,j} \longrightarrow C^{(ic)}_{i\,j} + W_{i\,\bar{i}}\,\bar{\bar{C}}^{(ca)}_{\bar{i}\,\bar{j}}\,U_{\bar{j}\,j}$$

expansion

complete *ic* resolution with indirect full *ca* span

$W_{i\,\bar{i}}$ is $\omega_i/\omega_{\bar{i}}$ if $i \in \bar{i}$ otherwise 0

$U_{\bar{j}\,j}$ is 1 if $j \in \bar{j}$ otherwise 0

2.4 Bundle-nS and Bundle-(Jp)nl projection

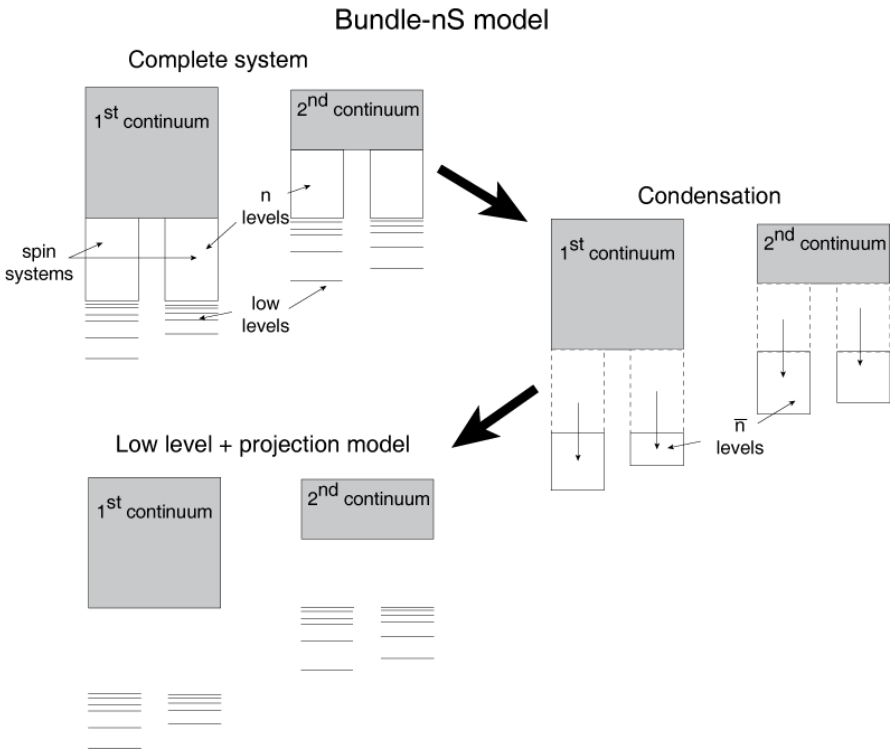

The projection/condensation system used by ADAS for light elements. Projection matrices are archived in format *adf17*. Mapping files are archived in *adf18*. (see also code ADAS204).

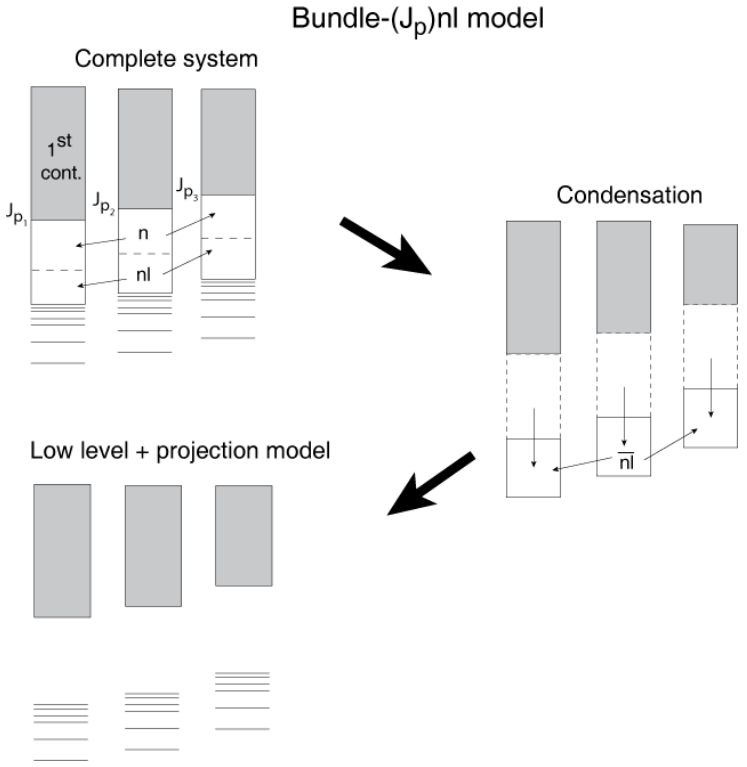

The projection/condensation system being completed by ADAS for medium-weight elements. It will also be used selectively for heavy elements

3.1 Ionisation state – the problem of heavy species

A heavy element such as tungsten with 74 ionisation stages overwhelms computer resources in 2-d impurity transport modelling. Typically elements with only up to about 15 ionisation stages can be handled.

Intermediate ions such as W^{+20} emit so many spectrum lines that they form a quasi-continuum. Almost none will ever be identified. A few ionisation stages (nearly closed shells or one or two electrons outside closed shells) emit simpler spectra with a modest number of strong lines.

The fractional ionisation potential change plot is helpful. The ionisation stages at and adjacent to the peak are the key stages for spectroscopy. They are the targets for the highest quality atomic modelling. Other ionisation stages might as well be grouped together, since they have narrow emission shells.

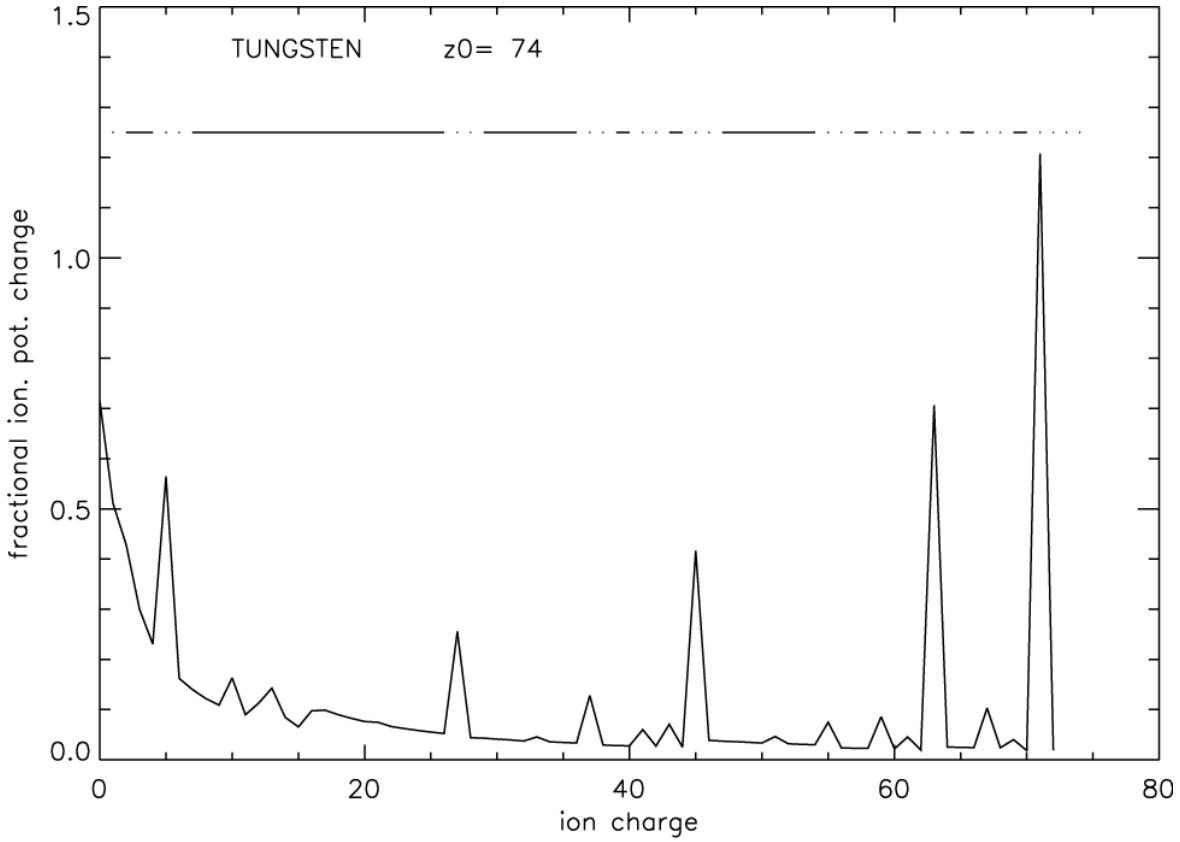

The broken bar at the top of the figure shows a possible grouping of ionisation stages, which also separates the individual spectroscopic stages. The process is called partitioning and the natural partition is shown for tungsten.

3.2 The new terminology and notation of superstages

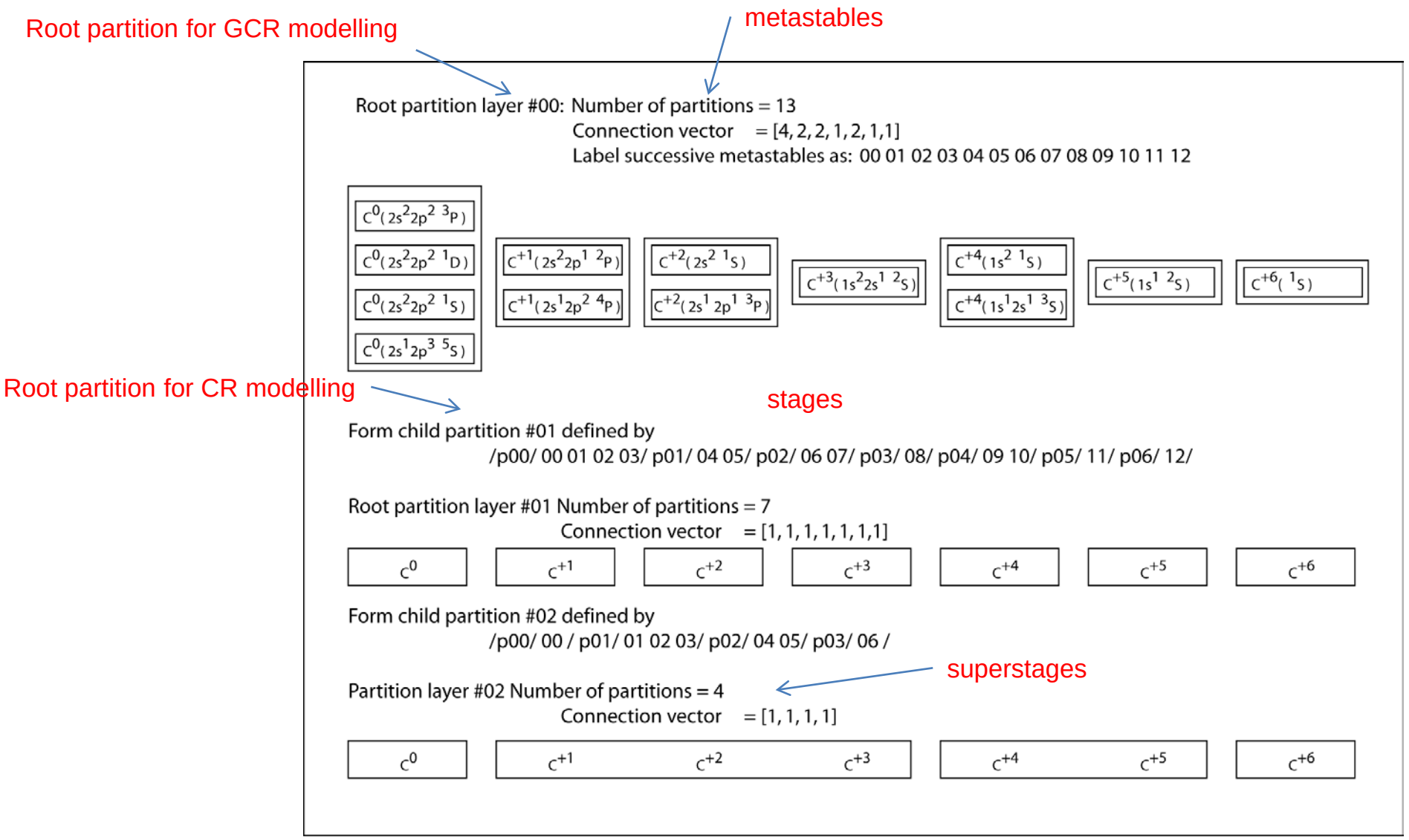

3.3 Algebra of superstage compression

$$N^{[\#02](j)} = \sum_{i=i_0}^{i_1} N^{[\#01](i)}$$

Partition j of layer #02 composed of partitions i_0 to i_1 of layer #01.

$$\frac{dN^{[\#02](j)}}{dt} = N_e S_{cr}^{[\#01](i_0-1\rightarrow i_0)} N^{[\#01](i_0-1)} - N_e \alpha_{cr}^{[\#01](i_0\rightarrow i_0-1)} N^{[\#01](i_0)} - N_e S_{cr}^{[\#01](i_1\rightarrow i_1+1)} N^{[\#01](i_1)} + N_e \alpha_{cr}^{[\#01](i_1+1\rightarrow i_1)} N^{[\#01](i_1+1)}$$

Sum time-dependent ionisation balance equations for partitions i_0 to i_1 of layer #01.

Impose equilibrium ratios on partitions i_0 to i_1 of layer #01.

$$N^{[\#01](i_0)}\Big|_{eq} = (\alpha_{cr}^{[\#01](i_0+1\rightarrow i_0)} / S_{cr}^{[\#01](i_0\rightarrow i_0+1)}) N^{[\#01](i_0+1)}\Big|_{eq}$$

$$N^{[\#01](i_0+1)}\Big|_{eq} = (\alpha_{cr}^{[\#01](i_0+2\rightarrow i_0+1)} / S_{cr}^{[\#01](i_0+1\rightarrow i_0+2)}) N^{[\#01](i_0+2)}\Big|_{eq}$$

$$\cdots$$

$$N^{[\#01](i_1-1)}\Big|_{eq} = (\alpha_{cr}^{[\#01](i_1\rightarrow i_1-1)} / S_{cr}^{[\#01](i_1-1\rightarrow i_i)}) N^{[\#01](i_1)}\Big|_{eq}$$

Gives definition of recombination and ionisation coeff-icients connecting j → j+1 and j → j-1 for layer #02.

$$\alpha_{cr}^{[\#02](j\rightarrow j-1)} = \alpha_{cr}^{[\#01](i_0\rightarrow i_0-1)} \left(N^{[\#01](i_0)} / N^{[\#02](j)}\right)\Big|_{eq}$$

$$S_{cr}^{[\#02](j\rightarrow j+1)} = S_{cr}^{[\#01](i_1\rightarrow i_1+1)} \left(N^{[\#01](i_1)} / N^{[\#02](j)}\right)\Big|_{eq}$$

Matrix algebra (see module 2 lecture notes) makes the handling simpler and universal.

Impurity transport modelling needs ionisation potentials, charge(z) and squared charge (z^2). For superstages these become collisional-radiative quantities, which vary with T_e and N_e written as: $\mathcal{ECD}$, $\mathcal{ZCD}$ and $\mathcal{YCD}$.

Some care is required with the formation energy of the first superstage – analogous to a work function (see the module 2 lecture notes).

Transport code have been modified to work with superstages.

3.4 ADAS adf11 dataset classes

ADF11 Subclass	Character	CR	GCR	Superstage
ACD	effective recombination coefft.	x	x	x
SCD	effective ionisation coefft.	x	x	x
CCD	effective CX recom. coefft.	(x)		(x)
PLT	effective excit. power coefft.	x	x	x
PRB	effective recom./brems. power coefft.	x	x	x
PRC	CX recom. power coefft.	(x)		(x)
QCD	effective metas. coupling coefft.		x	
XCD	effective parent metas. coupling coefft.		x	
ZCD	effective superstage charge			x
YCD	effective superstage squared charge			x
ECD	effective ionisation potential			x
ADF15 Subclass	Character			
$PEC^{(exc)}$	excit. photon emiss. coefft.	x	x	x
$PEC^{(rec)}$	recom. photon emiss. coefft.		x	
$FPEC^{(exc)}$	feature excit. photon emiss. coefft.			x
$FPEC^{(rec)}$	feature recom. photon emiss. coefft.			

3.5 adf11 datasets of different resolution and partition layers

adf11 datasets occur in up to 12 categories and in two basic forms. These forms are unresolved (CR), the upper case, and resolved (GCR), the lower two cases.

The partition specification may be omitted if it is the root partition of its form, that is #01 for unresolved and #00 for resolved.

The connection vector is required for the resolved form.

The lowest case has two partition layers, a child partition #01 and the resolved #00 root partition

The implementation of a superstage condensation is by the interactive code ADAS416, using a script from the user's ~/adas/scripts416/ directory. The script controls the *adf11* categories processed.

adf11 utilisation with simple ionisation stages or superstages is transparent to the user with superstage index s1 replacing ion charge number z1.

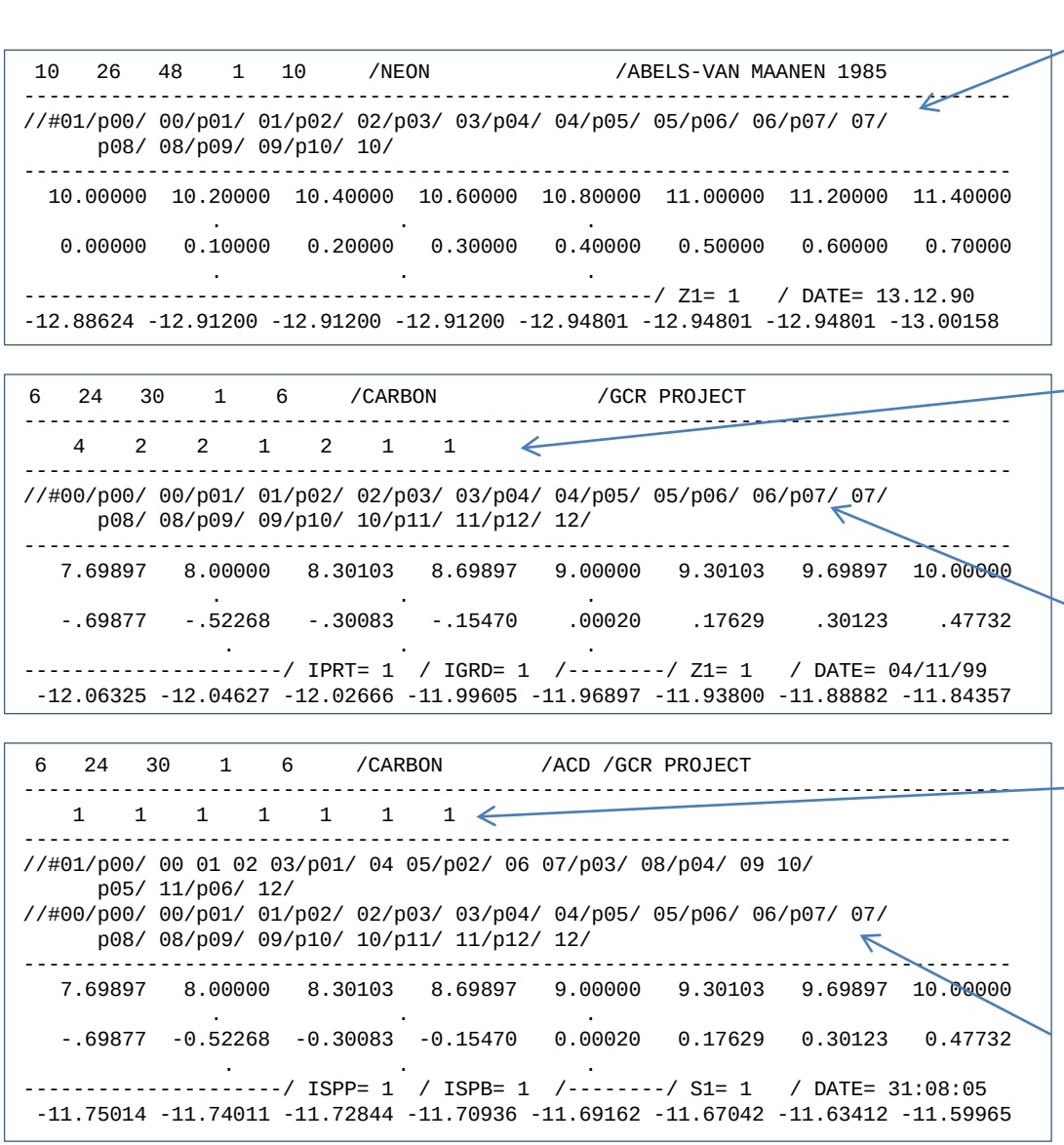

3.6 adf11 superstage coefficient behaviours

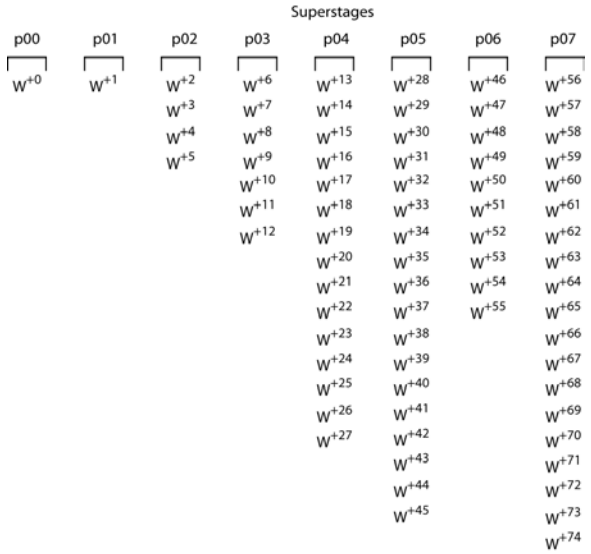

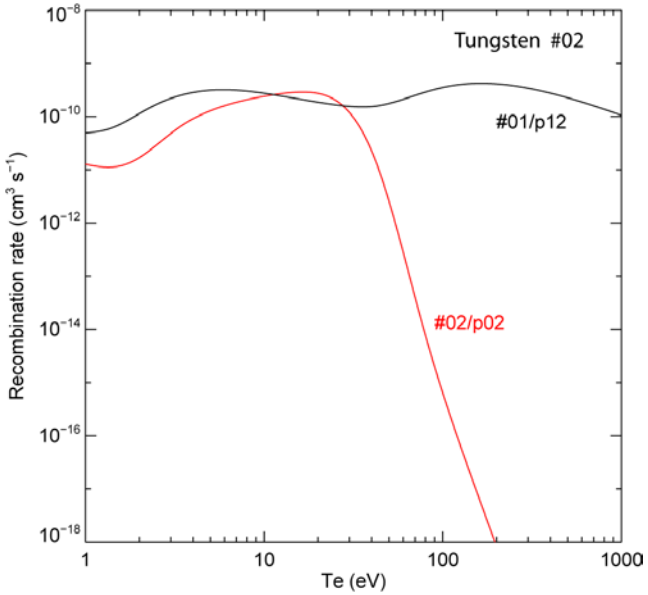

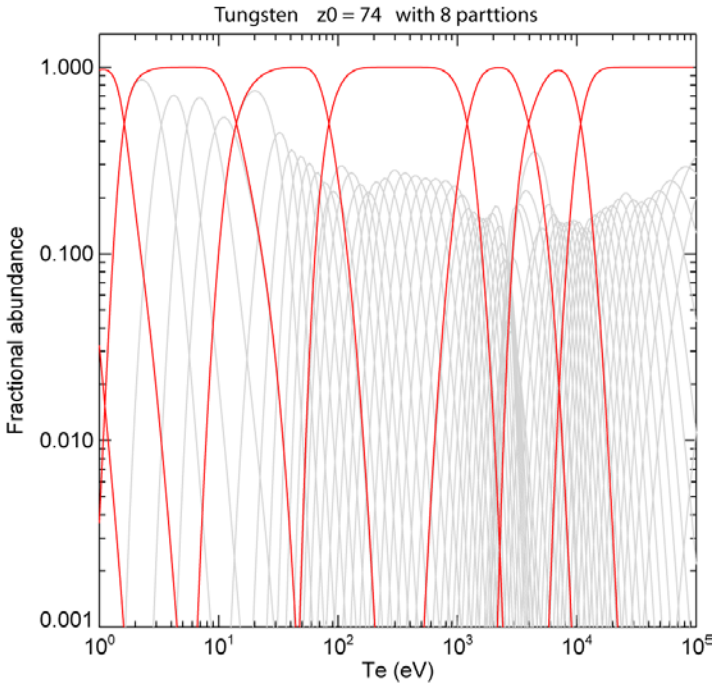

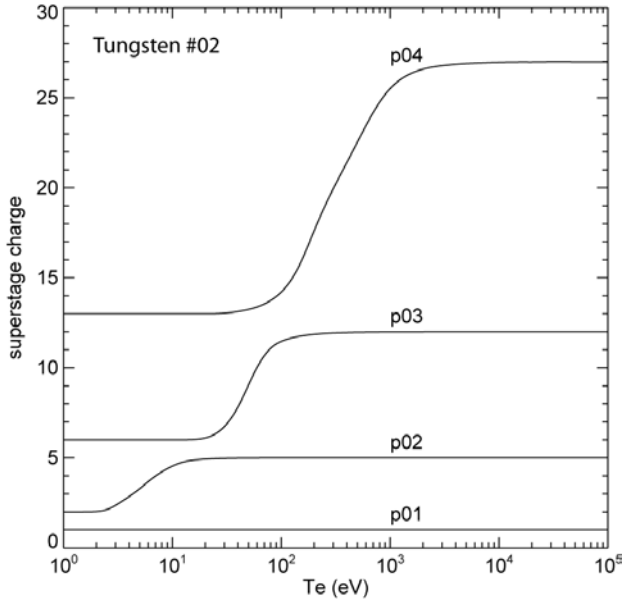

4.1 Population modelling for dielectronic resonance states

Zero-density doubly-excited state b-factors

$$b_{p,nl} = \left(\frac{\sum_{l'} A^{a}_{p,nl\to\nu' k' l'}}{\sum_{l'} A^{a}_{p,nl\to\nu k' l'} + A^{r}_{p,nl\to\nu',nl}} \right)$$

Finite density-corrected state-selective dielectronic coefficients using the BBGP approximation.

$$\alpha^{(d,IPIRDW)}_{\nu'\to\nu',nS}(N_e) = \alpha^{(d,IPIRDW)}_{\nu'\to\nu',nS}(N_e=0)\frac{\sum_l \alpha^{(d,BBGP)}_{\nu'\to\nu',nl}(N_e)}{\sum_l \alpha^{(d,BBGP)}_{\nu'\to\nu',nl}(N_e=0)}$$

Double-excited state population equations

$$\begin{aligned}
&-\left(N_e q^{e}_{nl-1\to nl} + N^{z_1} q^{z_1}_{nl-1\to nl}\right) N_{p,nl-1} \\
&+\left(\sum_{l'=l\pm1} N_e q^{e}_{nl\to nl'} + \sum_{l'=l\pm1} N^{z_1} q^{z_1}_{nl\to nl'} \right. \\
&\left. + \sum_{p_1=1}^{p-1} \sum_{l'=l-1}^{l+1} A^{a}_{p,nl\to p_1,\kappa l'} + \sum_{p_1=1}^{p-1} A^{r}_{p,nl\to p_1,nl} \right) N_{p,nl} \\
&-\left(N_e q^{e}_{nl+1\to nl} + N_{z_1} q^{z_1}_{nl+1\to nl}\right) N_{p,nl+1} \\
&= N_e \sum_{p_2=1}^{M} \sum_{l'=l-1}^{l+1} q^{c}_{p_2,\kappa l'\to p,nl} N_{p_2} + \sum_{p_1=p+1}^{P} A^{r}_{p_1,nl\to p,nl} N_{p_1,nl}
\end{aligned}$$

Ion impact coeffts.

Auger rate coeffts.

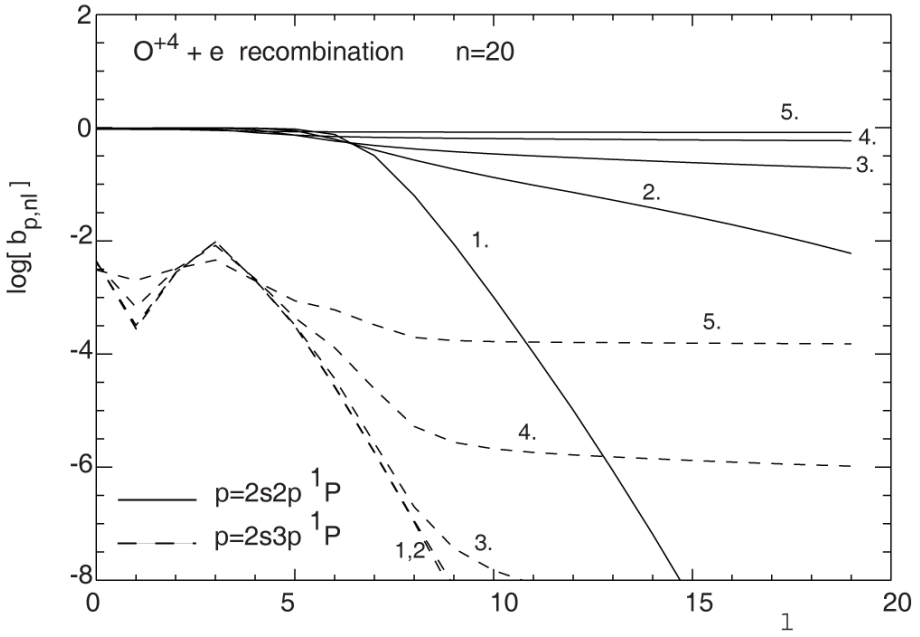

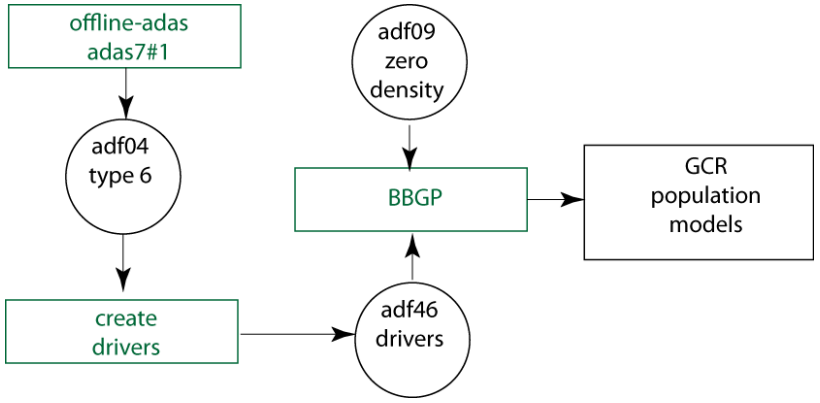

4.2 Impurity influx, ionisation pathways and photon efficiences.

The flux of an impurity is related to the number of ionisations from any ionisation stage along a line-of-sight to the surface which 'burns' through as it flows into the plasma from a surface. This provided there is no lateral loss and no return to the surface.

$$\Gamma^{\mathcal{A}} = \sum_{z=0}^{Z} \Gamma^{(z)}(0)$$

$$= \int_{\zeta=0}^{\infty} N_e \sum_{\sigma} \mathcal{SCD}_{\sigma}^{(Z\rightarrow Z+1)} N_{\sigma}^{(Z)}(\zeta) d\zeta$$

$$\mathcal{SCD}_{\sigma}^{(Z\rightarrow Z+1)} = \sum_{\nu'} \mathcal{SCD}_{\sigma\rightarrow\nu'}^{(Z\rightarrow Z+1)}$$

$$\Gamma^{\mathcal{A}} = \sum_{\sigma,\rho} N_e \left[\mathcal{SCD}_{\sigma}^{(Z\rightarrow Z+1)} W_{\sigma\rho}^{-1}\right] I_{\rho}$$

$\mathcal{SXB}_{\sigma\rho}$ ionisations per photon - another generalised-collisional-radiative quantity.

Observe a set of linearly independent spectrum lines equal to the number of metastables of stage Z.

$$\epsilon_{\rho} \equiv \epsilon_{\rho, i\rightarrow j} = \mathcal{PEC}_{\sigma, i\rightarrow j}^{(exc)} \sum_{k} C_{i,k}^{-1} \sum_{\sigma} C_{k\sigma} N_{\sigma}^{(Z)}$$

$$\epsilon_{\rho} = \sum_{\sigma} W_{\rho\sigma} N_{\sigma}^{(Z)}$$

$$N_{\sigma}^{(Z)} = \sum_{\rho} W_{\sigma\rho}^{-1} \epsilon_{\rho}$$

$$I_{\rho} = \int_{0}^{\infty} \epsilon_{\rho} d\zeta$$

4.3 Metastable resolved ionisation and SXB

ca resolution distorted wave ionisation cross-sections are the preferred ADAS general purpose source at this time. The *ls* resolution is deduced by a fractionation procedure.

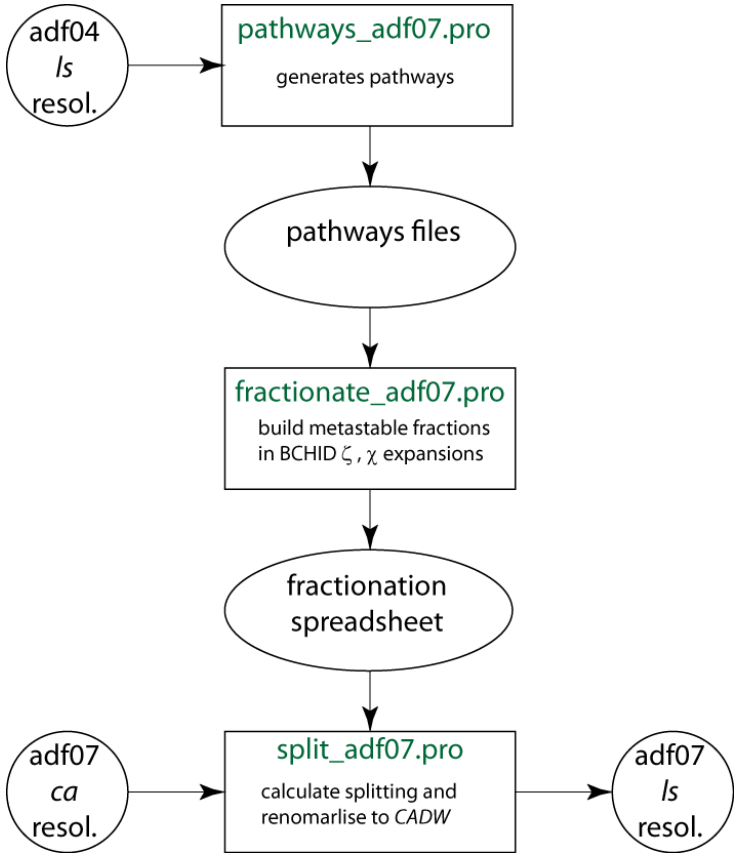

Details of fundamental data production are given in module 7.

The reciprocals of SXB coefficients are sometimes called photon efficiencies. The GCR version is necessary for valid influx estimation since metastables are not relaxed.

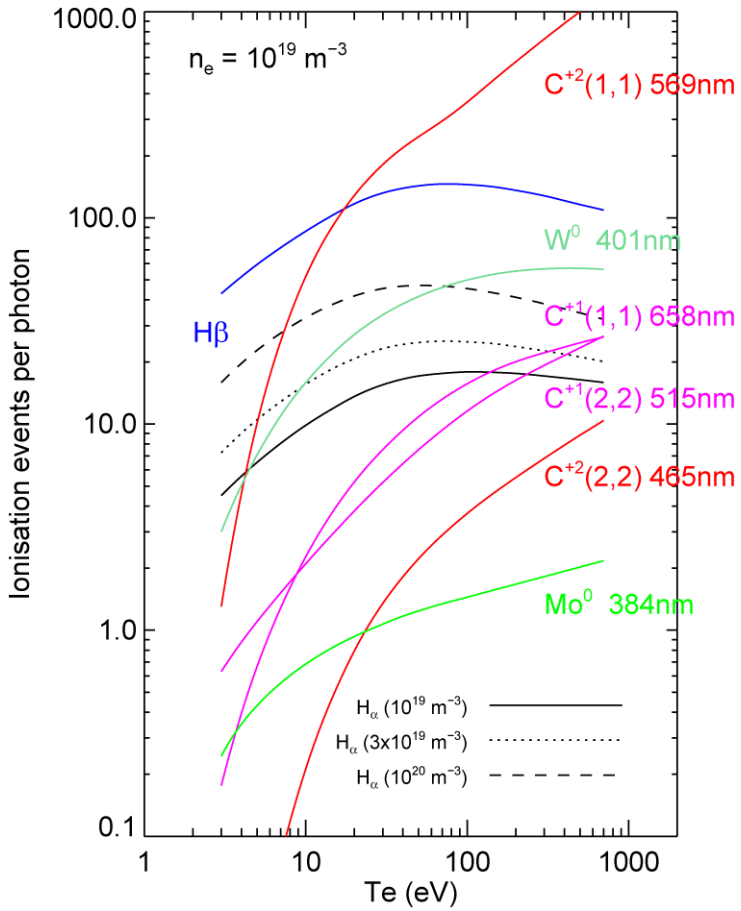

SXB has data format adf13. See *read_adf13.pro*.

5.1 Conclusions

- Population modelling has been described which can be used at various resolution levels, namely *ic*, *ls* and *ca*, depending on the availability of requisite *adf04* data sets. ADAS fundamental data production for medium/heavy species is tuned to these resolutions.

- The b_{nl} and b_n very high level population models in ADAS have been designed to solve the truncation problem such that their influence can be projected on the spans of the *adf04* datasets above.

- Progressive projection/condensation delivers necessary generalised collisional-radiative (*GCR*) spectroscopic data and plasma transport model data as data formats *adf11* and *adf15*.

- For heavy systems of great complexity, the technique of superstages and feature emisssivity coefficients (*adf40*) has been provided in ADAS, which allows attention to remain focussed on key ions, while still supporting full transport modelling.

- Extension of population modelling to dielectronic resonant states, via the bbgp method increases the precision to effective recombination and high densities.

- Inference of impurity influx, including testing of consistent influx from successive ionisation stages, from line-of-sight spectral observations is supported by ADAS in the full GCR framework, including a machinery for ionisation pathways through data classes *adf15* and *adf07*.

- More detail is given in the extended lecture-notes for module 2.